Surface tension and vapor–liquid phase coexistence of the square-well fluid

Jayant K. Singh, David A. Kofke, and Jeffrey R. Errington

Additional information on J. Chem. Phys.

Surface tension and vapor–liquid phase coexistence of the square-well fluid

Jayant K. Singh, David A. Kofke, and Jeffrey R. Errington
Department of Chemical Engineering, University at Buffalo, The State University of New York, Buffalo, New York 14260-4200

Vapor–liquid interfacial tension of square-well (SW) fluids is calculated using three different methods viz., molecular dynamics (MD) with collision-based virial evaluation, Monte Carlo with virial computed by volume perturbation, and Binder's density-distribution method in conjunction with grand-canonical transition-matrix Monte Carlo (GC-TMMC). Three values of the SW attractive well range parameter were studied: $\lambda = 1.5$, 1.75, and 2.0, respectively. The results from MD and GC-TMMC methods are in very good mutual agreement, while the volume-perturbation method yields data of unacceptable quality. The results are compared with predictions from the statistical associating fluid theory (SAFT), and SAFT is shown to give a good estimate for the systems studied. Liquid and vapor coexistence densities and saturation pressure are determined from analysis of GC-TMMC data and the results are found to agree very well with the established literature data. © *2003 American Institute of Physics.* [DOI: 10.1063/1.1590313]

I. INTRODUCTION

Interfacial properties are of fundamental interest in many technological processes. Understanding of interfacial behaviors can be aided by the application of theory and simulation to relatively simple model systems. These studies can uncover important qualitative features of interfaces that govern behavior in real systems. The most successful theoretical approach has been density functional theory,[1] and recently this technique has been applied with the statistical associating fluid theory (SAFT) treatment of associating fluids to consider effects of molecular association on interfacial properties.[2,3] One system studied in this manner is the square-well model, considering different ranges of attraction.[3] Assessment of the validity of this treatment can be aided by molecular simulation studies on the same model system.

There are several approaches for the study of vapor–liquid equilibrium by molecular simulation. Prominent examples include Gibbs ensemble Monte Carlo,[4] Gibbs–Duhem integration,[5] and NPT+test particle.[6] The results of these methods yield coexistence properties of the bulk phases, and as they are formulated in a way that does not put the phases in contact, they are unable to capture interfacial properties.

To study interfacial properties and structure, simulation of two coexisting phases within one simulation cell is necessary. Here the liquid-slab arrangement (Fig. 1) is the natural choice. This system is not commonly examined to evaluate bulk-phase properties because of concerns about the effect of the interface, and consequently the need for large system sizes to ensure that the bulk-phase behavior dominates, but it is widely used for studies of the interface itself. Even then, molecular simulation studies of interfaces are inherently inefficient, because the important behavior is contributed from the interfacial region only, which forms a relatively small portion of the entire system. Yet it is necessary to set up and simulate—with considerable expense—adjoining bulk phases which in some sense do not contribute to the properties of interest. This inefficiency seems to be unavoidable.

One concern in studies of interfaces is with the appropriate treatment of long-range contributions to the potential interactions, which should not be handled as in a bulk fluid because the density is inhomogeneous.[7–11] In the present study we skirt this issue by selecting to examine the square-well model, which itself is defined to have no long-range contributions.

The square-well (SW) model has been studied for decades. It is arguably the simplest model that incorporates both repulsive and attractive forces between molecules. The square-well potential is represented as

$$u(r_{ij}) = \begin{cases} \infty, & 0 < r_{ij} < \sigma, \\ -\varepsilon, & \sigma \leq r_{ij} < \lambda\sigma, \\ 0, & \lambda\sigma \leq r_{ij}, \end{cases}$$

where $\lambda\sigma$ is the potential-well diameter, ε is the depth of the well, and σ is the diameter of hard core. Because of its simplicity and analytic tractability the SW potential has been applied as a model of simple atomic systems,[12–14] colloidal particles,[15–17] heterochain molecules,[18,19] and complex system,[20–22] among others.

The rest of the paper is organized as follows: In the next section we briefly describe three methods used in this study for calculating the surface tension by molecular simulation. Section III describes the details of simulation conditions applied here. Section IV compares the results of surface tension obtained by the various methods and discusses the results of coexistence densities and vapor pressure. We conclude in Sec. V.
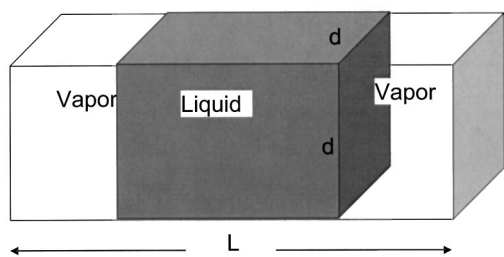
       3405

FIG. 1. Cartoon representing the initial simulation state for MC-volume change and molecular dynamics simulations.

II. SURFACE TENSION METHODOLOGIES

The conventional way of calculating surface tension by molecular simulation requires setting up a simulation cell as shown in Fig. 1. A slab of fluid is placed in a rectangular simulation cell with periodic boundaries, such that the fluid spans the short (x,y) dimensions of the simulation volume. The fluid is in contact with a vapor phase that fills the rest of the cell.

The thermodynamic definition of the surface tension γ expresses it in terms of the change in free energy F as the interfacial area A of two coexisting phases is changed at constant volume V,

$$\gamma = \left(\frac{\partial F}{\partial A}\right)_{T,V,N}. \tag{1}$$

From this definition one can show that the surface tension can be expressed in terms of components of the pressure tensor, such that for the geometry of Fig. 1,

$$\gamma = \tfrac{1}{2}\langle P_{ZZ} - \tfrac{1}{2}(P_{XX} + P_{YY})\rangle, \tag{2}$$

where $P_{\alpha\alpha}$ is the $\alpha\alpha$ component of the pressure tensor. The factor of $\tfrac{1}{2}$ multiplying the average accounts for the presence of two interfaces in the system. Two of the methods we use for the surface-tension calculation are based on this formula, and differ from each other in how the components $P_{\alpha\alpha}$ are measured.

A. Molecular dynamics

One way of calculating the pressure component is via the virial[23] for pairwise-additive potentials,

$$P_{\alpha\beta} = \rho kT + \frac{1}{V}\left\langle \sum_{i=1}^{N-1}\sum_{j>i}^{N}(\mathbf{r}_{ij})_{\alpha}(\mathbf{f}_{ij})_{\beta}\right\rangle, \tag{3}$$

where N is the number of molecules, ρ is the number density, k is the Boltzmann constant, T is the temperature, $\mathbf{r}_{ij}$ is the vector between the center-of-mass of molecules i and j, and $\mathbf{f}_{ij} = -\nabla u_{ij}$ is the force between them when their potential energy is u_{ij}; the angle brackets indicate an ensemble or time average. In the square-well model all forces are impulsive, having infinite magnitude but acting for an infinitesimal time. When integrated over time each collision contributes a well-defined amount to the average in Eq. (3),

$$P_{\alpha\beta} = \rho kT + \frac{1}{Vt_{\text{sim}}}\sum_{\text{collisions}}(\mathbf{r}_{ij})_{\alpha}(\Delta\mathbf{p}_{ij})_{\beta}, \tag{4}$$

where t_{sim} is the total simulation time and the sum is over all collisions occurring in this time; $\Delta\mathbf{p}_{ij}$ is the impulse associated with the collision between atoms i and j. The simulation proceeds in the usual manner for impulsive potentials:[23] solve for the time when the next pair collides (which occurs when any two particles reach a separation equal to the hardcore or square-well diameters), advance each particle to that time via free-flight kinematics, process the dynamics of the colliding pair, and move on to the next collision to repeat the process. With each collision a contribution to the pressure-tensor averages is made in accordance with Eq. (4).

B. MC-volume change

Calculation of the pressure-tensor components via Monte Carlo (MC) simulation is complicated by the impulsive nature of the contributions to the ensemble average. The singular contribution to the ensemble average has zero probability to be encountered in the sampling process, so instead the virial average must be computed by analysis of the cavity–cavity distribution function. Several distributions must be recorded to account for the different components of the pressure tensor.[24] We have not pursued this approach.

Instead we consider the measurement based directly on the definition of the pressure-tensor components in terms of derivatives of the free-energy with respect to the each dimension of the simulation cell. This derivative can be evaluated via free-energy perturbation methods. Harismiadis et al.[25] described a method of this type for measurement of the pressure in an isotropic system. Their method uses the finite-difference approximation,

$$\beta P = -(\partial\beta A/\partial V)_{T,N} \approx -[\beta A(V+\Delta V) - \beta A(V)]/\Delta V,$$

where P is the pressure, and the difference is measured via a straightforward free-energy perturbation (FEP) calculation.

In order to get pressure tensor components used in Eq. (2), we need two different kinds of volume perturbations. To get the P_{zz} component, we perform the volume change by perturbing only in the direction perpendicular to the interface, i.e., in the z direction. During this perturbation the area of the interface remains constant. To get $(P_{xx}+P_{yy})$, the component parallel to the interface, we apply volume change only in the direction parallel to x and y keeping the z dimension constant. During this perturbation, the width of the interface remains constant.

In an effort to improve the accuracy of the approach, we applied the overlap-sampling method[26] for the FEP calculation approach. In principle this requires we perform two independent simulations, one of the system of volume V perturbed to volume $V+\Delta V$, and a complementary one for a system of volume $V+\Delta V$ perturbed to volume V. The pressure is then

$$\beta P \approx \frac{N}{V} + \frac{1}{\Delta V}\ln\left[\frac{\langle\exp[-\beta(U(V+\Delta V)-U(V))/2]\rangle_V}{\langle\exp[-\beta(U(V-\Delta V)-U(V))/2]\rangle_V}\right]. \tag{5}$$

We applied an approximation in which the $V+\Delta V \rightarrow V$ calculation is given by a simulation of a system of volume V perturbed to one of volume $V-\Delta V$.

C. Grand-canonical transition-matrix Monte Carlo

The third route to the surface tension is based on the order-parameter distribution formalism of Binder.[27] Rather than set up an explicit interface, Binder's approach relies on spontaneous fluctuations that give rise to density inhomogeneities which provide information regarding the interfacial properties. Such an approach naturally lends itself to application near the critical point, where the necessary fluctuations are sufficiently large, and where maintenance of a well-defined interface causes difficulty for the explicit-interface methods. Until recently implementation of this method has been limited due to the difficulty of determining the density probability distribution required by the method. Errington[28] has shown how recent advances in sampling methodologies can be used to extend Binder's distribution-function method to conditions significantly away from the critical region. Another complication of Binder's method—the need to know the coexistence chemical potential—is alleviated by the related application of histogram reweighting.

At phase coexistence, the grand-canonical density probability distribution $P(\rho)$ attains a characteristic double peak structure.[29,30] The peaks correspond to stable (or metastable) homogeneous phases and the intermediate-density probability corresponds to a set of both homogeneous and heterogeneous configurations. As the system size becomes large, intermediate-density heterogeneous configurations far outweigh homogeneous ones, and the ratio of the density-probability distribution at the intermediate minimum relative to the (mutually equal) peak densities represents the interfacial free energy. Thus to calculate surface free energy one needs to determine the grand-canonical probability distribution $P(\rho)$ of finding the system at density $\rho = N/V$, for the thermodynamic state that satisfies the criteria for phase equilibrium.

Rather than work with the density distribution, it is more convenient conceptually and practically to consider the distribution of N at constant V. The distribution of N is described by a discrete probability distribution $\Pi_N = \Sigma_{s, N_s = N} \pi_s$, where π_s is a grand-canonical microstate probability, and the sum is over microstates for which the number of molecules is N. Specifically, for a chemical potential μ, temperature T (or inverse temperature $\beta = 1/kT$), and volume V, in the limiting distribution the Markov chain visits a given microstate s with a probability,

$$\pi_s = \frac{V^{N_s}}{\Xi \Lambda^{3N_s} N_s!} \exp[-\beta(U_s - \mu N_s)], \tag{6}$$

where U_s is the configuration energy, Ξ is the partition function, and Λ is the de Broglie wavelength.

The free energy of the interface for a finite-size system is determined from the maximum likelihood in the liquid $\Pi^l_{N\,\mathrm{max}}$ and vapor regions $\Pi^v_{N\,\mathrm{max}}$ and minimum likelihood in the interface region $\Pi_{N\,\mathrm{min}}$,

$$\beta F_L = \tfrac{1}{2}(\ln \Pi^l_{N\,\mathrm{max}} + \ln \Pi^v_{N\,\mathrm{max}}) - \ln \Pi_{N\,\mathrm{min}}.$$

From the formalism of Binder, the surface tension for a finite-size three-dimensional system is given by

$$\beta \gamma_L = \frac{\beta F_L}{2L^2} = C_1 \frac{1}{L^2} + C_2 \frac{\ln L}{L^2} + \beta \gamma_\infty,$$

where γ_∞ is the infinite system ($L \to \infty$) interfacial tension and C_1 and C_2 are constants. The expression suggests that the group $\beta F_L/2L^2$ becomes linear with scaling variable $\ln(L)/L^2$ as the system size approaches infinity. The method enables one to evaluate the infinite system interfacial tension by extrapolating a series of finite system calculations.

Away from the critical point, the probability to spontaneously sample intermediate densities is very small, and special measures must be applied to enable measurement of the probability distribution at these densities. The transition-matrix Monte Carlo (TMMC) (Ref. 31) method, with an N-dependent sampling bias, is well suited for this purpose. The method monitors the acceptance probability of attempted MC trials and subsequently uses this information to calculate the macrostate transition probability matrix. Once the transition probabilities are known, macrostate probabilities can be obtained from the detailed balance condition,

$$\Pi_N P_{N,N'} = \Pi_{N'} P_{N',N}. \tag{7}$$

The transition-probability matrix is tridiagonal, as the only transitions in N are such that $N \to N$, $N \to N+1$, and $N \to N-1$, so the set of Eqs. (7) yield unique values for the Π_N.

Biasing the simulation so that the system samples all states evenly requires setting a weight function $\eta(N)$ in accordance with multicanonical sampling.[32] In the present study, we set the weights equal to the inverse of current estimate of the macrostate probabilities, i.e.,

$$\eta(N) = -\ln \Pi(N).$$

As described above, in the TMMC approach we do not calculate directly the macrostate probabilities, but instead derive them from the macrostate transition probabilities. Accordingly, the weights are determined using the following sequential relation,

$$\eta(N+1) = \eta(N) + \ln\left(\frac{P_{N+1,N}}{P_{N,N+1}}\right),$$

where we take arbitrarily $\eta(0) = 0$. Acceptance criteria are modified in the presence of the bias as follows:

$$\mathrm{acc}(o \to n) = \min\left[1, \frac{\eta_n \pi_n}{\eta_o \pi_o}\right],$$

where η_n and η_o are weights corresponding to microstate n and o, respectively.

An advantage of the TMMC method is that it can be applied cumulatively, meaning that the existing transition-probability information does not need to be discarded upon redefinition of the sampling bias. This aspect of TMMC is helpful because the method relies on an iterative scheme to evolve the sampling bias, which ensures that all particle numbers are sampled sufficiently. By adopting this approach, new estimates of the bias reflect all transition-probability information collected from the onset of the simulation, and are not restricted to information taken only since the last update of the bias weights.
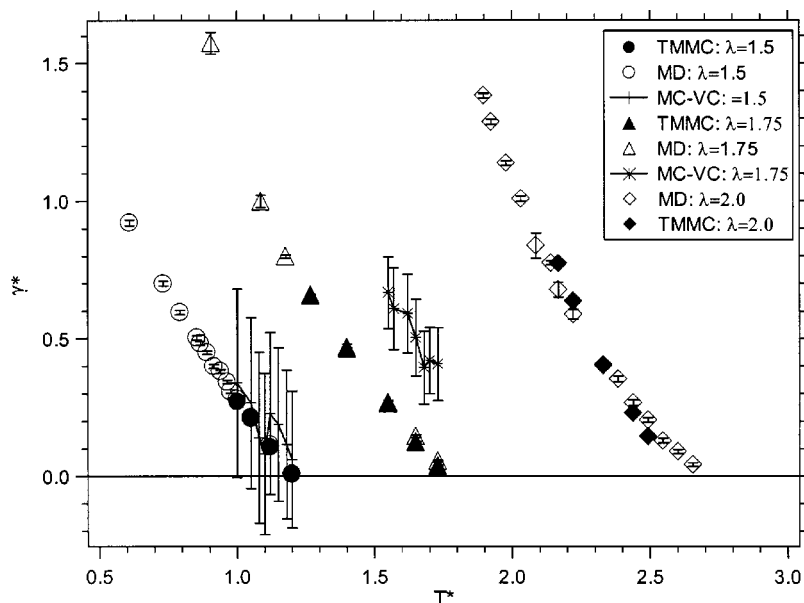
FIG. 2. Surface tension ($\gamma^* = \gamma\sigma^2/\varepsilon$) for the vapor–liquid interface of square-well fluid for three different well widths, as a function of temperature. Open symbols represent data via MD, filled symbols represent data via GC-TMMC, and lines are data via MC-volume change.

Another important element of this method is the use of the histogram reweighting method of Ferrenberg and Swendson[33] to evaluate the phase-coexistence value of the chemical potential. This determination is readily performed from knowledge of the probability distribution Π_N from the TMMC calculations. The probability distribution for any other chemical potential is calculated using the following relationship:

$$\ln\Pi(N;\mu) = \ln\Pi(N;\mu_o) + \beta(\mu - \mu_o)N,$$

where subscript "o" represents original simulation data. To determine the coexistence chemical potential, we apply the above relation to find the chemical potential that produces a probability distribution Π_N^{coex}, where the areas under the vapor and liquid regions are equal. Phase densities are calculated from the first moment of the Π_N^{coex} distribution.

Finally, to calculate the saturation pressure we use the following expression:[34]

$$\beta p V = \ln\left(\sum_N \Pi_N^{coex}/\Pi_0^{coex}\right) - \ln(2).$$

III. SIMULATION DETAILS

Vapor–liquid coexistence properties and surface tension for the square well model were computed using the methods described above. Three values of the square well parameter were studied: $\lambda/\sigma = 1.5$, 1.75, and 2.0.

A. Molecular dynamics

Our molecular dynamics (MD) simulations were performed in a canonical (NVT) ensemble, i.e., at prescribed particle number, volume, and temperature. The temperature was kept constant by simple momentum scaling, with all momenta multiplied by an appropriate factor at the end of each time step such that the total kinetic energy of the system is consistent with the equipartition value of the temperature.[23] The reduced time step Δt^* (in units of $\sigma\sqrt{m/\varepsilon}$) was fixed at 0.02; the only effect of the time-step

parameter is to determine the frequency for updating averages and rescaling velocities to the desired temperature. Otherwise the usual collision-based algorithm for generating molecule trajectories was employed.[23]

The simulation was started from a face centered-cubic lattice configuration in a cubic periodic box of dimension about 8.5 σ. We start with a density higher than the appropriate liquid density and expand the volume in one direction, extending it to four times its original value, to create the initial vapor region. The simulations were conducted with system sizes of 500 particles; a few simulations of 1024 particles (in a proportionately larger box) were performed at

TABLE I. Surface tension $\gamma^* = \gamma\sigma^2/\varepsilon$ as a function of temperature $T^* = kT/\varepsilon$ for square well molecules for three values of potential range (λ) evaluated via MD simulations of 500 particles. Numbers in parentheses indicate the 67% confidence limits of the last digit of the reported value.

$\lambda = 1.5$		$\lambda = 1.75$		$\lambda = 2.0$	
T^*	γ^*	T^*	γ^*	T^*	γ^*
0.88987	0.449(7)	1.0866	0.99(2)	1.897	1.382(8)
0.91425	0.398(7)	1.17715	0.799(5)	1.9241	1.286(9)
0.93863	0.381(6)	1.2677	0.655(5)	1.9783	1.137(7)
0.96301	0.342(6)	1.28581	0.632(5)	2.0325	1.007(9)
0.9752	0.307(6)	1.32203	0.570(5)	2.0867	0.83(4)
1	0.280(4)	1.35825	0.512(5)	2.1409	0.774(7)
1.05	0.213(4)	1.39447	0.463(5)	2.168	0.67(3)
1.08	0.171(3)	1.43069	0.420(5)	2.2222	0.58(1)
1.1	0.139(3)	1.4488	0.393(4)	2.3306	0.40(1)
1.12	0.115(3)	1.48502	0.352(5)	2.3848	0.35(1)
1.15	0.073(3)	1.52124	0.300(4)	2.439	0.265(9)
1.18	0.023(2)	1.55	0.268(4)	2.4932	0.203(9)
1.2	0.0074(20)	1.57	0.235(5)	2.5474	0.128(8)
		1.6	0.212(5)	2.6016	0.088(7)
		1.62	0.181(4)		
		1.65	0.145(4)		
		1.68	0.121(4)		
		1.7	0.079(3)		
		1.72	0.067(3)		
		1.73	0.055(3)		

TABLE II. Surface tension data of square well molecules with variable potential range (λ) of varying system size (cubic box of size L, in units of σ) from grand-canonical transition-matrix Monte Carlo and comparison with values from MD simulations. $T^* = kT/\varepsilon$. Numbers in parentheses indicate the 67% confidence limits of the last digit of the reported value.

	T^*	$L=8$	$L=9$	$L=10$	$L=12$	$L=14$	$L=\infty$	MD
$\lambda = 1.5$	1	0.252(2)	0.258(2)	0.263(2)	0.268(10)	0.273(9)	0.288(7)	0.280(4)
	1.05	0.175(1)	0.179(1)	0.186(2)	0.190(10)	0.196(9)	0.209(5)	0.213(4)
	1.12	0.085(1)	0.087(1)	0.088(1)	0.093(1)	0.097(1)	0.107(2)	0.115(3)
	1.2	0.0161(2)	0.0156(5)	0.0143(5)	0.0126(7)	0.0118(12)	0.0068(13)	0.0074(20)
$\lambda = 1.75$	1.268	0.614(1)	0.623(2)	0.629(4)	0.636(1)	0.670(6)	0.658(3)	0.656(6)
	1.55	0.203(1)	0.210(1)	0.217(2)	0.230(1)	0.238(2)	0.264(3)	0.268(4)
	1.65	0.101(1)	0.102(1)	0.105(1)	0.110(1)	0.114(1)	0.124(2)	0.145(4)
	1.73	0.043(1)	0.041(1)	0.040(1)	0.039(1)	0.040(2)	0.037(1)	0.055(3)
$\lambda = 2.0$	2.2222	0.456(1)	0.484(1)	0.508(1)	0.548(1)	0.561(2)	0.636(1)	0.58(1)
	2.3306	0.290(1)	0.306(1)	0.317(1)	0.350(1)	0.367(1)	0.401(2)	0.40(1)
	2.439	0.102(1)	0.154(1)	0.181(1)	0.191(1)	0.204(3)	0.228(1)	0.265(9)
	2.4932	0.115(1)	0.117(1)	0.120(1)	0.128(1)	0.136(2)	0.144(2)	0.203(9)

lower temperatures to ensure there were no significant finite-size effects. The simulations were equilibrated for 1 million time steps and averages were taken for 1 million time steps.

B. MC-volume change

The scheme used to generate the interface in the MD simulations is also used for MC. The simulations were performed in a NVT ensemble with system sizes again of 500 or 1024 particles. The simulations were equilibrated for 700 K MC cycles and averages were taken for 500 K MC cycles, where one MC cycle is N MC trials. The volume change step was taken in $\ln V$ and was fixed for the simulation to range across ± 0.0005 for all the cases.

C. GC-TMMC

We performed grand-canonical-transition matrix Monte Carlo simulations with frequency 90% particle insertion/deletion and 10% particle displacements. Bias weights $\eta(N)$ were updated after every million MC trials. The length of the runs ranged from 300 million to one billion trials, depending on the simulation box size. Four independent simulations were performed for calculating the confidence limits. Coexistence properties were calculated using a cubic box of size 10 σ. Surface tensions were calculated using the finite size scaling method, with cubic boxes of size $L=8$, 9, 10, 12, and 14σ. In order to speed up the calculation a cell-based neighbor list scheme was applied. The data of del Rio *et al.*[35] gave a good indication of the coexistence value of the chemical potential, and this value was input to the GCMC simulations. For temperatures different from those studied by del Rio *et al.*, we interpolated their values.

IV. RESULTS AND DISCUSSIONS

Figure 2 presents results using methods discussed above for the surface tension of the SW model for three well widths, as a function of temperature. Table I presents the surface tension data via MD, and Table II presents the data of surface tension for different system size via GC-TMMC and a comparison of values via MD. The MC volume change

method performs very poorly in this application, with confidence limits that are 70–120 times larger than those for the MD and GC-TMMC calculations (which themselves are in excellent mutual agreement). Also, the MC volume change results at the largest well width $\lambda = 1.75$ diverge from the other results at higher temperatures. The results from the volume-change method do not seem to have a useful level of precision and accuracy, particularly in comparison to the other techniques, and thus we will not further consider the results from this method. GC-TMMC results are shown only for $T/T_c \geq 0.82$, $T/T_c \geq 0.7$, $T/T_c \geq 0.8$ for the potential range $\lambda = 1.5$, 1.75, and 2.0, respectively. Below temperature $T/T_c = 0.7$, the GC-TMMC approach used here (which considers the entire range of density in one sampling window) has difficulty in sampling the entire vapor–liquid region, mainly because of the large differences in the free energies across the range of states leads to longer simulation length for the convergence of weights (in a subsequent study on a different system we have parallelized this algorithm, with sampling performed in individual windows across the den-
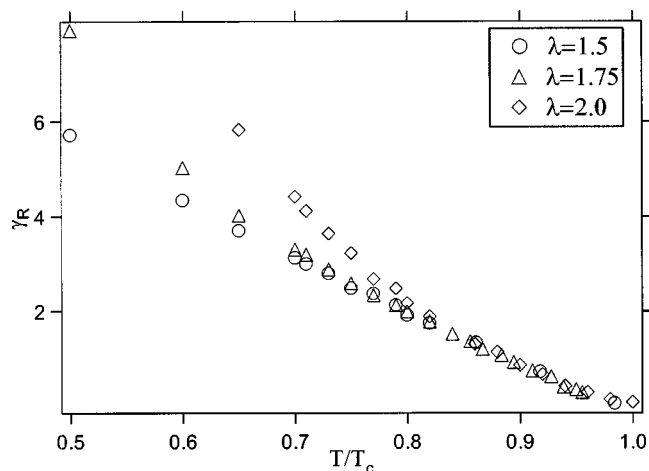

FIG. 3. Vapor–liquid surface tension of the square-well model of various well-extents λ in corresponding state form. γ_R represents reduced surface tension ($\gamma \rho_c^{1/3}/p_c$). T_c is the critical temperature. The values are calculated via molecular dynamics. The error bars are smaller than the symbol size.

TABLE III. The critical temperature T_c^*, density ρ_c^*, and pressure P_c^* data for square-well fluids with variable potential range λ estimated from grand-canonical transition-matrix Monte Carlo and rectilinear diameter approach and compared with literature values.

λ	T_c^*	ρ_c^*	P_c^*	Source
1.5	1.2172(7)	0.3079(2)	0.0931(3)	This work
	1.2180(2)	0.310(1)	0.095(1)	Orkoulas et al.[a]
	1.218	0.3016	0.0939	del Rio et al.[b]
	1.27	0.305577	0.11	Elliot et al.[c]
	1.219(8)	0.299(23)	0.108(16)	Vega et al.[d]
1.75	1.809(2)	0.2653(18)	0.1263(11)	This work
	1.808	0.2648	0.1276	del Rio et al.[b]
	1.79	0.26738	0.12	Elliot et al.[c]
	1.811(13)	0.284(9)	0.179(20)	Vega et al.[d]
2.0	2.68(1)	0.251(26)	0.1975(43)	This work
	2.691	0.2549	0.2021	del Rio et al.[b]
	2.61	0.26738	0.17	Elliot et al.[c]
	2.764(23)	0.225(18)	0.197(26)	Vega et al.[d]

[a]Reference 36.
[b]Reference 35.
[c]Reference 37.
[d]Reference 13.

sity range, and find that the GC-TMMC method can be made much more effective at lower temperatures). Unsurprisingly, there are enhanced system-size effects upon approach of the critical temperature, and the MD results overestimate the more accurate (due to finite-size scaling) GC-TMMC results. Figure 3 presents the data (excluding the MC results) in corresponding-states form, with surface tension and temperature reduced by the critical-point density and temperature: $T_R = T/T_c$, $\gamma_R = \gamma \rho_c^{1/3}/P_c$. The critical properties themselves are reported in Table III.

The data show that, as expected, the surface tension increases with well extent λ and decreases with temperature, approaching a value of zero at the critical point. When viewed in reduced form, the surface tension is invariant with the range of the potential for T_R greater than 0.8, at least for the three cases considered here. At lower reduced temperatures, the plots show more curvature, with the effect becom-
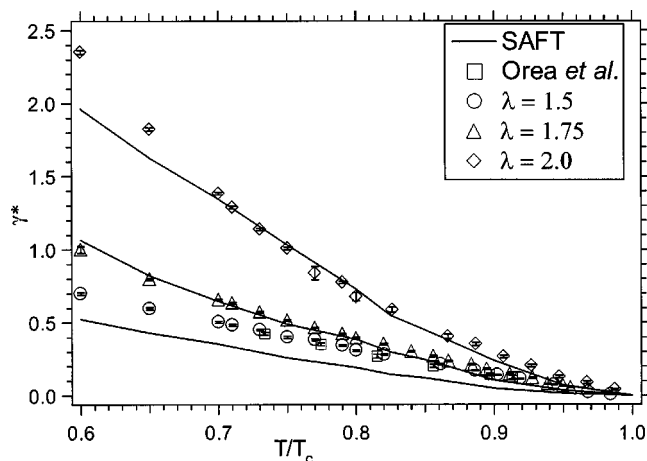
TABLE IV. Vapor–liquid coexistence data from grand-canonical transition-matrix Monte Carlo simulations of square well molecules with variable potential range ($\lambda = 1.5, 1.75, 2.0$). Subscripts v and l represents vapor and liquid, respectively. The errors in densities and pressures represent one standard deviation of the mean for four independent runs.

T^*	ρ_v^*	ρ_l^*	P^*
$\lambda = 1.5$			
0.8533	0.0097(1)	0.7162(1)	0.0075(1)
1	0.0315(1)	0.646(1)	0.0251(1)
1.05	0.0453(1)	0.6187(4)	0.03526(2)
1.08	0.05639(5)	0.5999(6)	0.04277(2)
1.1	0.06550(1)	0.5846(5)	0.04843(1)
1.12	0.0762(1)	0.567(2)	0.05461(3)
1.15	0.0971(2)	0.5384(1)	0.06500(3)
1.18	0.1298(2)	0.4965(5)	0.07707(4)
1.2	0.1641(4)	0.456(2)	0.08622(2)
$\lambda = 1.75$	1	0.0019(1)	0.725(9)	0.0019(1)
1.2	0.00811(2)	0.6643(7)	0.00894(2)
1.268	0.01199(3)	0.641(2)	0.01357(2)
1.3	0.01409(2)	0.629(2)	0.0161(2)
1.5	0.03706(6)	0.555(1)	0.04236(2)
1.55	0.0462(1)	0.5343(5)	0.0519(1)
1.57	0.0505(1)	0.5252(4)	0.0561(1)
1.6	0.0579(1)	0.5107(2)	0.06299(8)
1.62	0.0633(1)	0.5020(4)	0.06786(7)
1.65	0.0729(1)	0.4848(7)	0.0757(1)
1.68	0.0844(1)	0.4677(4)	0.08419(2)
1.7	0.0934(1)	0.4558(8)	0.09018(4)
1.72	0.1049(3)	0.4384(5)	0.09670(4)
1.73	0.1115(6)	0.431(1)	0.1000(1)
1.75	0.1278(9)	0.4106(8)	0.1071(1)
1.8	0.217(18)	0.381(8)	0.12786(7)
$\lambda = 2.0$	1.897	0.0111(5)	0.71(1)	0.0192(5)
2.1	0.0247(4)	0.636(8)	0.0432(6)
2.2	0.03465(3)	0.598(1)	0.05992(9)
2.35	0.05489(4)	0.5339(2)	0.09101(7)
2.45	0.07467(3)	0.4872(3)	0.1168(1)
2.5	0.0878(2)	0.4624(8)	0.13145(1)
2.52	0.0945(1)	0.4517(1)	0.1378(1)
2.53	0.0973(2)	0.4468(7)	0.1408(1)
2.54	0.1011(4)	0.441(1)	0.1442(2)
2.56	0.1094(1)	0.4274(7)	0.1508(1)
2.57	0.1137(2)	0.423(1)	0.1541(1)

FIG. 4. A comparison of surface tension computed via MD with the results of Orea et al. (Ref. 24) and with the results of SAFT as calculated by Gloor et al. (Ref. 3).

ing increasingly pronounced for increasing potential range, and causing the curves to diverge from one another.

Figure 4 shows a comparison of the present MD results with SAFT calculations of Gloor et al.[3] for the same SW potential models. We have interpolated the results of Gloor et al. to get the surface tension values for $\lambda = 1.5$ and $\lambda = 1.75$. For the shortest-range system, the SAFT results consistently underestimate the surface tension, but are in excellent agreement with simulation for $\lambda = 1.75$; this agreement deteriorates as λ is increased to 2.0, but only at the lowest temperatures. Overall the SAFT treatment does a good job in describing the effect of temperature and potential range on the surface tension. The plot also shows a very good agreement for $\lambda = 1.5$ with the simulation results of Orea et al.[24]

The results from the GC-TMMC method are sufficient to calculate in detail the orthobaric densities and vapor pressure for SW fluids at each well width at several temperatures. The results of this calculation are reported in Table IV and in
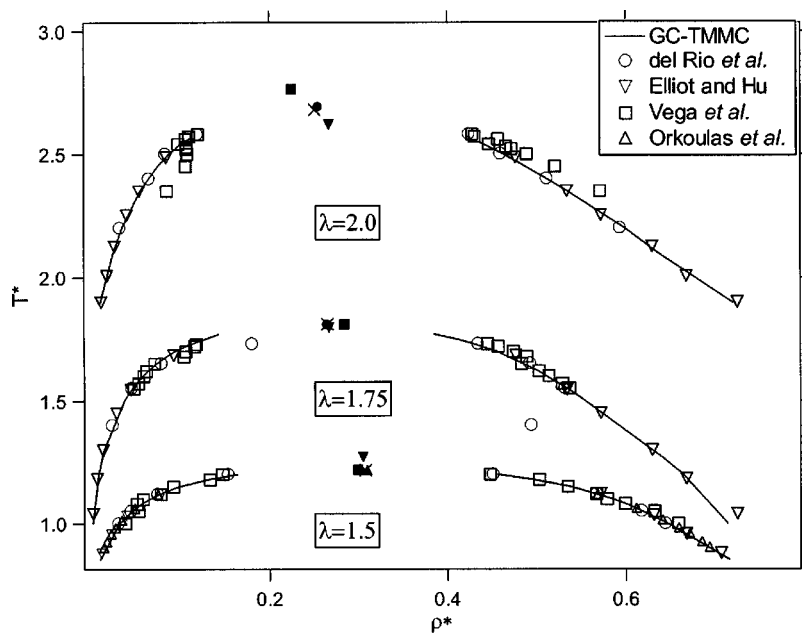
FIG. 5. Orthobaric densities of the square-well model for three values of the well extent λ, measured via TM-GCMC and compared with the results of del Rio *et al.* (Ref. 35), Elliot and Hu (Ref. 37), Vega *et al.* (Ref. 13), and Orkoulas *et al.* (Ref. 36). The critical point estimated by GC-TMMC (marked by the ×) is also displayed and compared with literature values.

Fig. 5, where they are compared with previous results of del Rio *et al.*,[35] Orkoulas and Panagiotopoulos,[36] Elliot and Hu,[37] and Vega *et al.*[13] In all cases the new GC-TMMC results are quite precise for all conditions studied, even near the critical temperature. The agreement with del Rio *et al.* is excellent, aside from one point that appears to reflect a typographical error in Ref. 35. Results from Elliot *et al.* are in quite good agreement too, except at one liquid point (low temperature) for potential range λ = 1.75 and 2.0. In comparison, the data of Vega *et al.* look flawed, a conclusion also made by del Rio *et al.* We compare our results of potential range λ = 1.5 additionally with the calculations of Orkoulas *et al.* The agreement there is excellent, as it is with all the other studies for this system, suggesting all these methods perform well for this system.

Figure 6 shows the saturated vapor pressure in a Clausius–Clapeyron plot, as calculated via GC-TMMC. Comparison with the literature data follows the same trends

as with the orthobaric densities: the agreement is very good, except for the Gibbs ensemble data of Vega *et al.*[13]

The critical properties are estimated from a least square fit of the law of rectilinear diameter and the scaling relation,[38]

$$\rho^l - \rho^v = C_1 \left(1 - \frac{T}{T_c} \right)^{\beta_c} + C_2 \left(1 - \frac{T}{T_c} \right)^{\beta_c + \Delta},$$

where ρ^l and ρ^v are the liquid and vapor densities, respectively, and C_1 and C_2 are fitting parameters. The critical exponent β_c is taken as 0.325 and $\Delta = 0.51$. The critical temperature estimate from the above is utilized to get the critical density from the least square fit of the following expression:
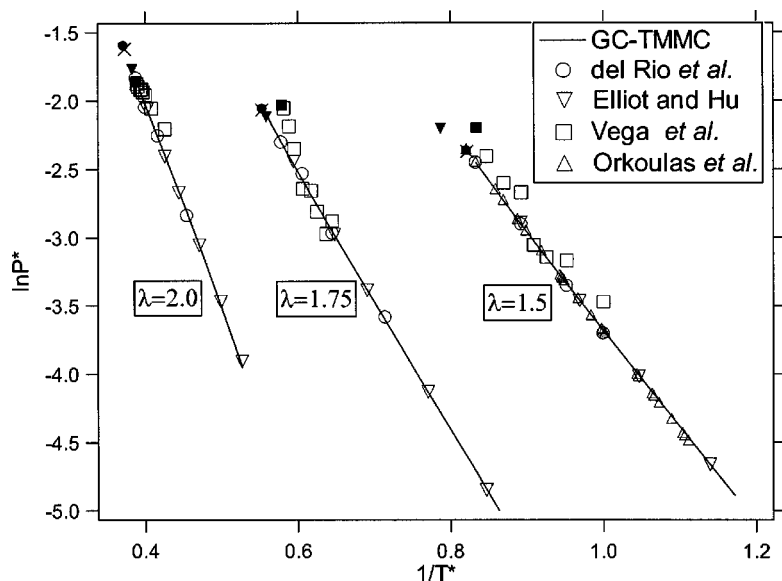
$$\frac{\rho^l + \rho^v}{2} = \rho_c + C_3 (T - T_c).$$

FIG. 6. The vapor pressure curve for the square-well fluids for three values of the well-extent λ. The results of this work are shown with the other literature values. Also shown are the critical points (×) from the GC-TMMC compared with the estimates of del Rio *et al.* (Ref. 35), Elliot and Hu (Ref. 37), Vega *et al.* (Ref. 13), and Orkoulas and Pangiotopoulos (Ref. 36) (for λ = 1.5).

Critical pressure is calculated using the least square fitting of the following expression:

$$\ln P = A + B/T,$$

where A and B are constants.

The critical properties of the square well fluid with variable range of well-width are listed in Table I. We compared the critical value estimation with the results of del Rio et al.,[35] Orkoulas and Panagiotopoulos,[36] and Elliot and Hu.[37] Our results are in good agreement with del Rio et al.[35] and Orkoulas and Panagiotopoulos.[36] The critical points estimated by Elliot and Hu[37] show some deviation from the current results.

V. CONCLUSION

We compared the interfacial tension of the square-well model as calculated with several techniques, and for several values of the attractive range of the potential. We found that MC-volume change is not a good method for this system. GC-TMMC and MD are in good mutual agreement. We also compared the surface tension calculated via GC-TMMC/MD with SAFT, and concluded that SAFT gives a good estimate of square-well surface tension.

Based on our experience in this work and studies currently underway, we consider the MD method to be better for the surface tension calculation of the SW system when applied at low temperatures ($T < 0.7T_c$), and that the GC-TMMC method with finite-size scaling is better at higher temperatures. However our overall preference is for the GC-TMMC method, as we have since found that it can be parallelized well, making it effective over the entire range of fluid conditions. This observation holds *a fortiori* when the methods are applied for even more complex systems, such as models for associating fluids.

In addition to surface tension calculation, we also presented phase coexistence data which are given with high precision using GC-TMMC method. Critical properties are also estimated and are found to be in good agreement with results reported recently by del Rio *et al.*

ACKNOWLEDGMENTS

[1] R. Evans, Adv. Phys. **28**, 143 (1979); J. Winkelmann, J. Phys.: Condens. Matter **13**, 4739 (2001); H. Lowen, *ibid.* **14**, 11897 (2002).

[2] F. J. Blas, E. M. del Rio, E. de Miguel, and G. Jackson, Mol. Phys. **99**, 1851 (2001).

[3] G. J. Gloor, F. J. Blas, E. M. del Rio, E. de Miguel, and G. Jackson, Fluid Phase Equilib. **194–197**, 521 (2002).

[4] A. Z. Panagiotopoulos, Mol. Phys. **61**, 813 (1987).

[5] D. A. Kofke, Mol. Phys. **78**, 1331 (1993).

[6] D. Moller and J. Fischer, Mol. Phys. **69**, 463 (1990); A. Lofti, J. Vrabec, and J. Fischer, *ibid.* **76**, 1319 (1992); D. Moller and J. Fischer, *ibid.* **75**, 1461 (1992).

[7] E. M. Blokhuis, D. Bedeaux, C. D. Holcomb, and J. A. Zollweg, Mol. Phys. **85**, 665 (1995).

[8] M. Guo, D.-Y. Peng, and B. C.-Y. Lu, Fluid Phase Equilib. **130**, 19 (1997).

[9] M. Guo and B. C.-Y. Lu, J. Chem. Phys. **106**, 3688 (1997).

[10] M. Mecke, J. Winkelmann, and J. Fischer, J. Chem. Phys. **107**, 9264 (1997).

[11] A. Trokhymchuk and J. Alejandre, J. Chem. Phys. **111**, 8510 (1999).

[12] F. Del Rio and D. A. Delonngi, Mol. Phys. **56**, 691 (1985).

[13] L. Vega, E. de Miguel, L. F. Rull, G. Jackson, and I. A. McLure, J. Chem. Phys. **96**, 2296 (1992).

[14] J. Chang and S. I. Sandlar, Mol. Phys. **81**, 745 (1994).

[15] P. Bolhuis and D. Frenkel, Phys. Rev. Lett. **72**, 2211 (1994).

[16] N. Asherie, A. Lomakin, and G. B. Benedek, Phys. Rev. Lett. **77**, 4832 (1996); M. G. Noro and D. Frenkel, J. Chem. Phys. **113**, 2941 (2000).

[17] E. Zaccarelli, G. Foffi, K. A. Dawson, F. Sciortino, and P. Tartaglia, Phys. Rev. E **63**, 031501 (2001).

[18] J. Cui and J. R. Elliot, J. Chem. Phys. **114**, 7283 (2001).

[19] C. McCabe, A. Gil-Villegas, G. Jackson, and F. Del Rio, Mol. Phys. **97**, 551 (1999).

[20] A. Lomakin, N. Asherie, and G. B. Benedek, J. Chem. Phys. **104**, 1646 (1996).

[21] Y. Zhou, M. Karplus, K. D. Ball, and R. S. Berry, J. Chem. Phys. **116**, 2323 (2002).

[22] Y. Zhou, M. Karplus, J. M. Wichert, and C. K. Hall, J. Chem. Phys. **107**, 10691 (1997).

[23] M. P. Allen and D. J. Tildesley, *Computer Simulation of Liquids* (Clarendon, Oxford, 1987).

[24] P. Orea, Y. Duda, and J. Alejandre, J. Chem. Phys. **118**, 5635 (2003).

[25] V. I. Harismiadis, J. Vorholz, and A. Z. Panagiotopoulos, J. Chem. Phys. **105**, 8469 (1996).

[26] N. Lu, J. K. Singh, and D. A. Kofke, J. Chem. Phys. **118**, 2977 (2003).

[27] K. Binder, Phys. Rev. A **25**, 1699 (1982).

[28] J. R. Errington, Phys. Rev. E **67**, 012102 (2003).

[29] T. L. Hill, *Thermodynamics of Small Systems, Parts I and II* (Dover, New York, 1962).

[30] J. J. Potoff and A. Z. Panagiotopoulos, J. Chem. Phys. **112**, 6411 (2000).

[31] M. Fitzgerald, R. R. Picard, and R. N. Silver, Europhys. Lett. **46**, 282 (1999).

[32] B. A. Berg and T. Neuhaus, Phys. Rev. Lett. **68**, 9 (1992).

[33] A. M. Ferrenberg and R. H. Swendsen, Phys. Rev. Lett. **61**, 2635 (1988).

[34] J. R. Errington and A. Z. Panagiotopoulos, J. Chem. Phys. **109**, 1093 (1998).

[35] F. Del Rio, E. Avalos, R. Espindola, L. F. Rull, G. Jackson, and S. Lago, Mol. Phys. **100**, 2531 (2002).

[36] G. Orkoulas and A. Z. Panagiotopoulos, J. Chem. Phys. **110**, 1581 (1999).

[37] J. R. Elliot and L. Hu, J. Chem. Phys. **110**, 3043 (1999).

[38] L. J. Van Poolen, C. D. Holcomb, and V. G. Niesen, Fluid Phase Equilib. **129**, 105 (1997).